J. Fluid Mech. (1978), *vol.* 86, *part* 2, *pp.* 247–271
Printed in Great Britain

Experiments on buoyant-parcel motion and the generation of internal gravity waves

By CARMEN P. CERASOLI

Geophysical Fluid Dynamics Program, Princeton University,
Princeton, New Jersey 08540

(Received 1 July 1976 and in revised form 19 September 1977)

Laboratory experiments were conducted to study the motion of miscible buoyant fluid parcels in both homogeneous and stratified media, and were complemented with numerical experiments using the model of Orlanski & Ross (1973). Parcel motion in the homogeneous case was found to be shape-preserving, in agreement with the large body of data for such motion. The stratified medium experiments were such that the parcel attained equilibrium positions. It was found that the time for the parcel to reach maximum depth was approximately 0·7 times the buoyancy period, independent of that depth. The subsequent collapse of the parcel and generation of internal gravity waves was observed. Ray-like patterns of waves propagated out from the collapse region, and wave frequencies near 0·7 times the Brunt–Väisälä frequency were predominant. The internal wave energy radiated away from the collapsed parcel was estimated and found to be 20 to 25 % of the change in the system potential energy.

1. Introduction

The existence of internal gravity waves in the free atmosphere has been well established and their importance appreciated. The effects of internal gravity waves in the atmosphere are many and varied; they may affect mesoscale weather features, generate clear-air turbulence and cause ionospheric disturbances. One source of internal waves is penetrative convection, and this paper describes experiments performed to study this particular generation process.

The motion of miscible fluid parcels was observed in both a homogeneous and a stratified fluid. Parcel motion in a homogeneous fluid has received considerable attention from laboratory experimenters (Scorer 1957; Richards 1963; Turner 1964), while similar studies for parcel motion in a stratified fluid are less common. Morton, Taylor & Turner (1956) performed laboratory studies of parcel motion in a stratified fluid to identify and verify the variables which determined the parcel penetration distance. McLaren *et al.* (1973) studied the problem of internal gravity wave generation by buoyant parcels, with a particular emphasis on using wave information to determine the source location. Orlanski & Ross (1973) carried out a numerical experiment for the motion of an isolated thermal in a stratified fluid using a model designed to simulate gravity waves and turbulent processes. That study demonstrated the effectiveness of penetrative convection as a source of internal waves.

The experimental apparatus and techniques are described in §2. The laboratory results are presented in §3, while a simple entraining parcel model is discussed in §4,

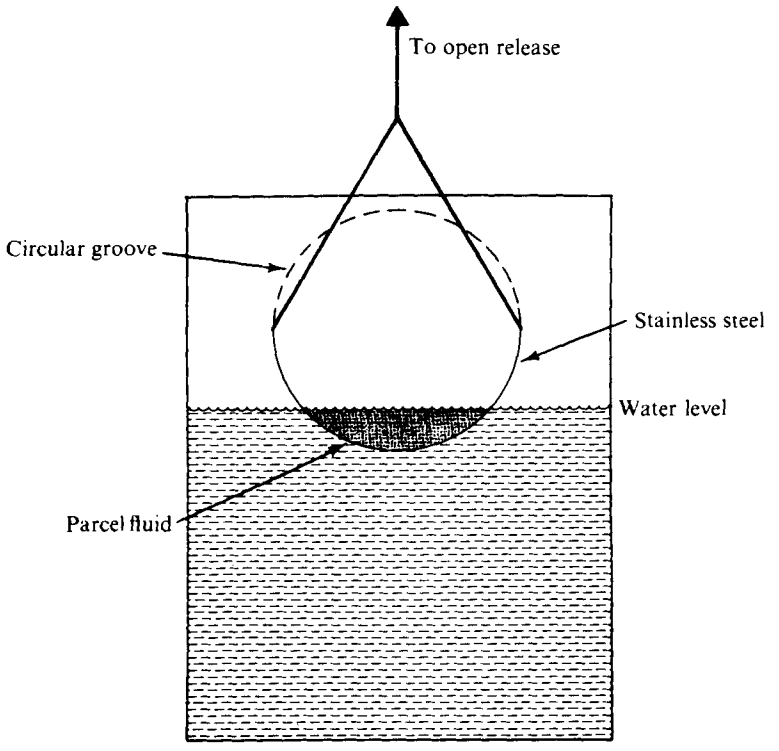

FIGURE 1. Schematic diagram of parcel dropper, used to introduce the parcel into the main body of fluid.

along with an explanation of the observed wave field. The numerical model is described in §5, and results from numerical experiments are compared with laboratory data. Finally, a summary and discussion are presented in §6.

2. Experimental apparatus and techniques

Apparatus

The experiments were performed in a Plexiglas tank 150 cm long, 89 cm deep and 28 cm wide. A brine solution was the ambient fluid for the stratified flow experiments and stratification was obtained by a method similar to that of Fortuin (1960). The details of the filling apparatus and procedure are described by Delisi & Orlanski (1975). The tank was filled to a depth of approximately 80 cm and salinity versus depth profiles were linear to within 5 % throughout this depth. Fresh water occupied the uppermost centimetre, minimizing the effect of evaporation and surface mixing of the linear density region. Densities at the bottom of the tank ranged from approximately 1·015 to 1·050 g cm^{-3}, which resulted in corresponding buoyancy periods of about 15 to 8 s.

A parcel of salty water was introduced across the width, and at the top of the tank; this resulted in average parcel motions which were two-dimensional. The device for introducing the parcel, shown in figure 1, consisted of two thin (1·6 mm) stainless steel quarter-cylinders held in circular grooves. The cylinders were placed with one long side of each touching the other and lightweight grease was used to provide a water-tight

seal. The device was positioned at the top of the tank and filled with a prescribed amount of saline solution. The quarter-cylinders were opened simultaneously, thus introducing the parcel into the main body of the fluid. The cylinders opened in about one tenth of a second, which created a small amount of mixing. The mixing caused solely by the cylinder motion was observed by filling the parcel dropper with dyed fluid of ambient density and opening the cylinders. Instabilities associated with the shear created by the cylinder motion were observed at the dye interface, and were the cause of mixing and growth of the dyed fluid. This growth was far less rapid (typically, size doubled in 5 to 10 s) than the growth of a falling parcel due to entrainment. The dyed fluid did not translate downward, indicating that no significant mean circulation was created. That is, the cylinder motion did not produce a vortex pair.

Experiments were performed both with and without wave absorbers at the vertical side walls. The absorbers were punched Plexiglas plates with 1·3 cm diameter holes spaced every 1·9 cm, and placed about 4 cm from the vertical wall. Delisi & Orlanski (1975) found that for waves with horizontal and vertical wavelengths of approximately 20 cm, the absorbers reduced the vertical component of the reflected wave by nearly a factor of three. In the present study, a spectrum of wavelengths is excited, with lengths typically about 30 to 40 cm. The efficiency of the absorbers decreases with wavelength and it is doubtful that the reflected wave is reduced by better than 50 % for these wavelengths. For larger scale waves (of the order the tank size), the absorbers are almost completely ineffective.

Techniques

Salinity (and therefore density) measurements were made using conductivity probes. The use of these probes in the laboratory has become fairly standard and is discussed by Maxworthy & Browand (1975). The conductivity gauge and probe system was calibrated using an American optical refractometer to measure salinity, and probes were used to determine both mean and fluctuating densities. Four probes could be operated simultaneously, while d.c. amplifiers were used to amplify the low-level, fluctuating conductivity-gauge outputs. A Honeywell Instrument tape recorder was also used to record conductivity-gauge outputs.

Blue Dextran dye was added to the saline solution at regular intervals during the filling to produce thin, evenly spaced dye lines with a vertical spacing of about 4 cm. Dye was usually added to the fluid parcel and the tank was illuminated from behind. Typically, two motor-driven 35 mm cameras were used; one was triggered at either two or four frames per second to follow the parcel motion, while the other was usually triggered at one frame per second to photograph the internal wave motion. Streak photography of neutrally buoyant particles was used in some experiments. This technique requires side lighting of the tank, so a fluorescing dye was used when simultaneous dye and streak photographs were required.

3. Experimental results

Parcel motion in a homogeneous fluid

Figures 2 and 3 are examples of the two photographic techniques used in this study. The tank is illuminated from behind in figure 2 (plate 1) and the dye provides a fairly

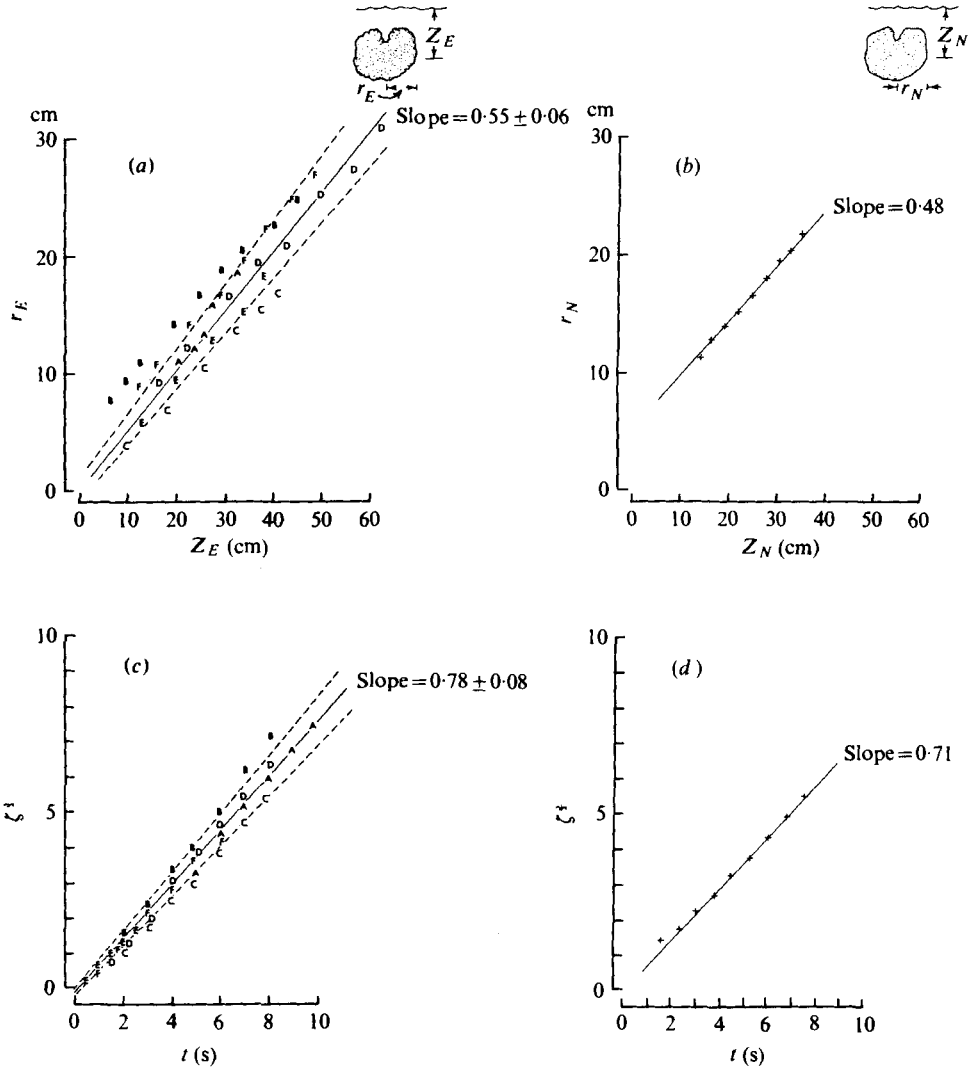

FIGURE 4. (*a*) Parcel radius as a function of vertical position from a number of laboratory experiments. (*b*) The variable z_E raised to the two-thirds power as a function of time for the same experiments given in (*a*). $\zeta_E \equiv z_E(gB_0A_0)^{\frac{1}{3}}$. For *A*, $B_0 = 0{\cdot}010$, for *B*, $B_0 = 0{\cdot}053$, for *C*, $B_0 = 0{\cdot}107$, for *D*, $B_0 = 0{\cdot}140$, for *E*, $B_0 = 0{\cdot}182$, for *F*, $B_0 = 0{\cdot}197$. $A_0 = 22{\cdot}4$ cm^2. (*c*) and (*d*) are similar to (*a*) and (*b*), respectively, except that the data were derived from numerical experiment. $\zeta_N \equiv z_N/(gB_0A_0)^{\frac{1}{3}}$.

sharp outline with which to define the parcel. A typical set of streak photographs is shown in figure 3 (plate 2), where fluorescent dye was added to the parcel. The half second exposure time is not short enough to identify streaks with instantaneous streamlines, but does indicate the vortex pair nature of the parcel motion.

The vertical midpoint of the dyed region with respect to the free surface was measured, along with parcel width (see illustration in figure 4) for a number of experiments. It was found that the parcel radius r_E (defined as one half parcel width) was proportional to the vertical position z_E and that

$$z_E \sim (gB_0A_0)^{\frac{1}{3}}t^{\frac{2}{3}}.$$

B_0 is defined as $$B_0 \equiv (\rho_I - \rho_0),$$

where ρ_I and ρ_0 are the initial parcel density and ambient density, and the subscript E indicates experimental values. A_0 is the initial parcel area (volume divided by tank width), g is the acceleration of gravity and t is time measured from the opening of the parcel dropper.

The results from this set of experiments are given in figures 4(*a*) and (*b*). Parcel radius was plotted versus position in figure 4(*a*) and it was found that

$$r_E = \alpha z + r_0,$$

with $$\alpha = 0{\cdot}55 \pm 0{\cdot}06,$$

and $$r_0 = -0{\cdot}6 \pm 1{\cdot}0 \text{ cm}.$$

It has been suggested that α (the entrainment coefficient) is a function of B_0 (see Escudier & Maxworthy 1973), but the present experiment was not sensitive enough to detect any systematic variation of α with B_0. In figure 4(*b*), the variable $\zeta_E^{\frac{3}{2}}$ ($\zeta_E \equiv z_E/(gB_0A_0)^{\frac{1}{3}}$) is plotted as a function of time for a range of initial parcel densities, and it was found that

$$\zeta_E^{\frac{3}{2}} = k_E t + \zeta_0^{\frac{3}{2}},$$

with $$k_E = 0{\cdot}78 \pm 0{\cdot}08,$$

and $$\zeta_0^{\frac{3}{2}} = 0{\cdot}20 \pm 0{\cdot}14 \text{ s}.$$

Parcel motion in a linearly stratified fluid

Photographs of a typical experiment are presented in figure 5 (plate 3), illustrating a number of features of parcel motion and the generation of internal gravity waves. Time is measured from the release of the parcel in units of the buoyancy period T, defined as

$$T = 2\pi/N,$$

where $$N^2 = \frac{g}{\rho_a}\frac{d\rho_a}{dz},$$

and $\rho_a(z)$ is the ambient density with z measured positive downward. The initial phase of parcel motion, figure 5(*a*), $t = 0{\cdot}26T$, is similar to the parcel motion in a homogeneous fluid. A vortex pair is formed and the parcel radius increases linearly with vertical position. In figure 5(*b*), $t = 0{\cdot}44T$, the parcel continues to fall, but begins to flatten as a result of the ambient stratification inhibiting vertical motions. During this stage, the effect of the vortex pair motion can be seen behind the parcel, with isopycnics being distorted up and down around into the back of the parcel. Isopycnics ahead of the parcel are being forced downward at this time. The front of the parcel reaches maximum depth in figure 5(*c*), $t = 0{\cdot}7T$, which coincides with the maximum displacement of isopycnics just below the parcel. Ambient fluid then moves upward, collapsing the parcel, as shown in figure 5(*d*), $t = 0{\cdot}96T$. Figure 5(*e*), $t = 1{\cdot}84T$, and figure 5(*f*), $t = 2{\cdot}45T$, show the internal gravity wave field after parcel collapse, where ray-like patterns emanating from the collapse region can be discerned.

The position of the parcel front, z_f, was measured relative to the free surface as a function of time for a number of experiments. It was found that the maximum depth, Z_m, was always reached in approximately $0{\cdot}7T$, independent of B_0 and A_0, where B_0

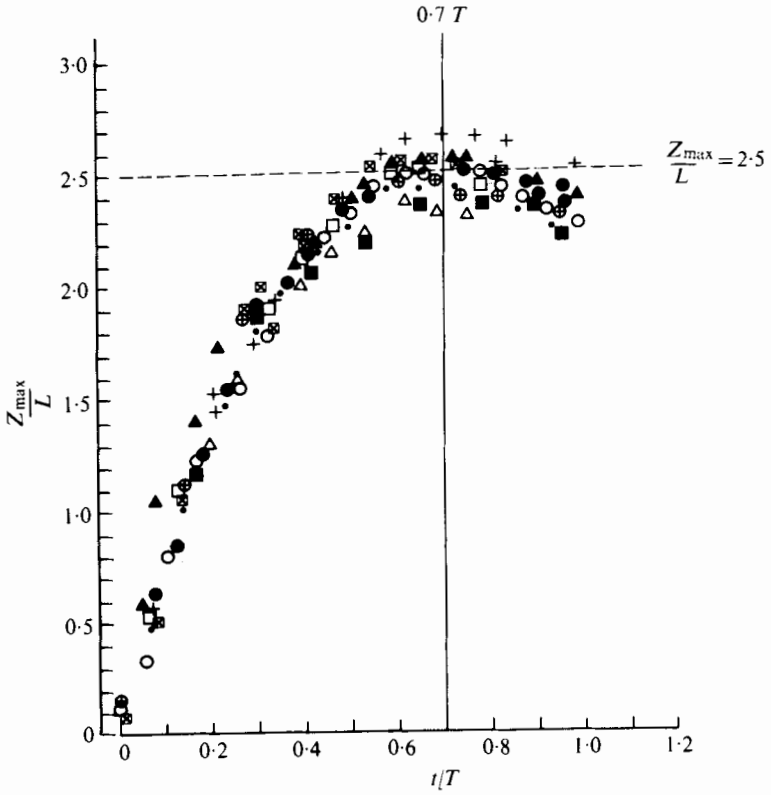

FIGURE 6. Parcel position as a function of time for a number of experiments with a linearly stratified fluid. Parcel position has been normalized by $L \equiv (gB_0A_0\frac{1}{4}N^2)^{\frac{1}{4}}$ and time by $T \equiv 2\pi N$. +, $B_0 = 0{\cdot}038$, $T_0 = 13{\cdot}0$ s; ○, $B_0 = 0{\cdot}076$, $T_0 = 13{\cdot}0$ s; ⊕, $B_0 = 0{\cdot}114$, $T_0 = 13{\cdot}0$ s; •, $B_0 = 0{\cdot}054$, $T_0 = 10{\cdot}9$ s; □, $B_0 = 0{\cdot}083$, $T_0 = 10{\cdot}9$ s; ⊠, $B_0 = 0{\cdot}110$, $T_0 = 10{\cdot}9$ s; ▲, $B_0 = 0{\cdot}088$; $T_0 = 7{\cdot}7$ s; ●, $B_0 = 0{\cdot}176$, $T_0 = 7{\cdot}7$ s.

ranged from approximately 0·01 to 0·16 and A_0 equalled 12·1 and 24·2 cm². Z_m was found to be proportional to the length scale L, defined as

$$L = \left(\frac{gB_0A_0}{N^2}\right)^{\frac{1}{4}}.$$

This result follows directly from dimensional arguments if one assumes that the maximum parcel depth depends only upon the initial parcel mass per unit width, $\rho_0 B_0 A$, and the ambient stratification, $d\rho_a/dz$. (ρ_0 was taken as $\rho_a(z = 0)$ and was always equal to 1·000.)

Data from a number of experiments are presented in figure 6, where z_f/L is plotted as a function of t/T. The initial parcel area was kept fixed at 12·1 cm² (corresponding to a volume of 350 cm³) and the values of B_0 and T are given in the legend. The values of $\rho_0 B_0$ ranged from approximately 2 to 8 times the difference between the ambient density at the top and bottom of the tank. Such values of B_0 may appear to be large, but were necessary for the parcel to obtain a significant Z_m. This is a consequence of the efficient turbulent entrainment of ambient fluid, which rapidly decreases the parcel's density. The data of figure 6 show that Z_m is approximately $2{\cdot}5L$ and is reached in about $0{\cdot}7T$ after release. Similar results are true for the position of the parcel centre,

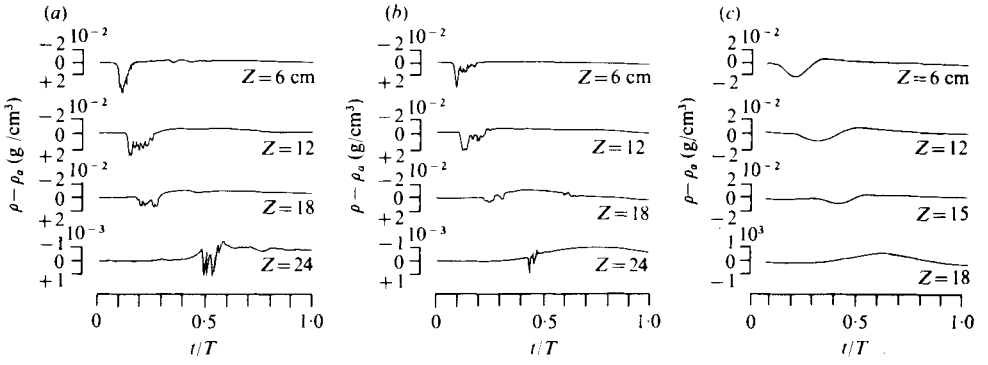

FIGURE 7. Data in (*a*) and (*b*) give density deviation from ambient at four vertical positions along tank centre-line as a function of normalized time for two similar laboratory experiments. Data show the passage of the dense parcel fluid. (*c*) is similar except that data were derived from numerical experiment.

defined as the vertical midpoint of the dyed region. It was found that the maximum centre position was approximately $1{\cdot}8L$ and attained in about $0{\cdot}7T$ also.

Conductivity-probe measurements recorded the parcel motion; data from two similar experiments are shown in figures 7 (*a*) and (*b*). The probes were placed on the centre-line $x = 0$ of the tank at 6, 12, 18 and 24 cm from the free surface. Differences between the two sets of records are discernible and will be discussed. The similarities between records will be dealt with first.

At the 6 cm probe, the parcel passes as a dense, compact entity with a maximum density of approximately 1·050. At the 12 cm position, a weak response before the passage of the parcel is just discernible, which represents the downward motion of of isopycnics ahead of the parcel. The maximum density at this position is approximately 1·020 g cm^{-3}, and given that the initial parcel density was 1·120 g cm^{-3}, the efficiency of the mixing processes can be appreciated. The signal following the passage of dense fluid results from ambient fluid at levels above the probe being advected into the area by the vortex pair motion. At the 18 cm position, the qualitative features of the two records agree, where one observes the initial downward isopycnic motion, and the passage of dense fluid followed by light fluid advected from above. The records at the 24 cm position show both a response from the downward isopycnic motion and spikes due to parcel fluid. The parcel density is now greatly reduced and the magnitude of the spikes represents fluid with a density excess of about 0·002 g cm^{-3} over the ambient.

The quantitative differences between the two sets of records result from asymmetries produced by the parcel dropper. This causes the path of the parcel's centre not to coincide with the tank centre-line, so that probes placed on the tank centre-line will not sample precisely the same region of the parcel from one experiment to another. Inspection of the accompanying photographs shows that for the first experiment, the parcel centre was slightly off centre-line, while the second experiment had them more closely aligned. Despite this limitation of the data, they show qualitative features and provide an estimate of the magnitude of the parcel density during its descent.

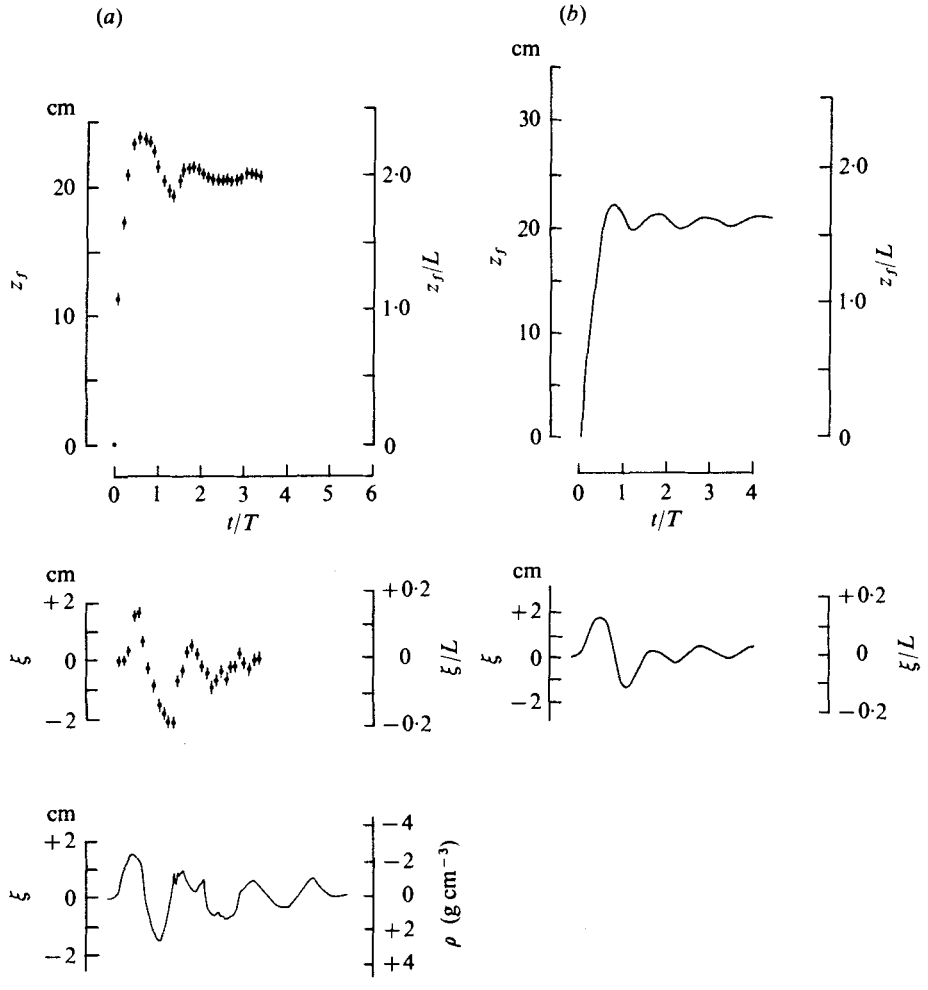

FIGURE 8. (*a*) illustrates the following variables as a function of normalized time: parcel front position z, dye line displacement for an isopycnic approximately 2 cm below maximum parcel position Z_m, and conductivity probe output for a probe placed approximately 2 cm below Z_m. (*b*) shows parcel front position and isopycnic displacement for position about 2 cm below Z_m as a function of normalized time for data derived from numerical experiment.

Internal gravity waves

The parcel motion and the ambient fluid response are coupled, as evidenced in figure 5(*d*), where the disturbance excited by the parcel in turn collapses the parcel. This coupling can be observed in figure 8(*a*), where the following variables are plotted as a function of time for a standard experiment:† parcel position z_f/L, isopycnic displacement ξ/L for a dye line approximately 2 cm below Z_m, and the conductivity probe signal for a probe placed at approximately Z_m. All three measurements were taken at the centre-line ($x = 0$) of the tank. Both the probe and dye line data indicate that the isopycnics near Z_m reach maximum displacement at approximately $0{\cdot}7T$,

† A standard experiment is one with $A_0 = 12{\cdot}1$ cm^2 and $\rho_0 B_0$ equal to twice the density difference between the top and bottom of the tank. This initial condition yielded $Z_m \sim 30$ cm independent of the ambient stratification.

coinciding with the time of maximum parcel penetration. The subsequent oscillations with a period of about $1{\cdot}4T$ can be most clearly seen in the probe and parcel data. One full oscillation can be observed in the dye line data, but after this, measurements become unreliable as the dye diffuses owing to the large amplitude. The density measurement ρ' gathered from the probe data is related to the isopycnic displacement ξ_p by the linear relation

$$\xi_p = \frac{\rho'}{d\rho_a/dz}. \tag{3.1}$$

The maximum displacement of isopycnics directly below Z_m was approximately $0{\cdot}15L$, independent of L for values ranging from 10 to 25 cm, and the characteristic amplitude of the waves propagating away from the collapse region was also about $0{\cdot}15L$. Parcel radius (or size) before collapse was approximately L, and wave amplitudes were typically 0·10 to 0·15 times parcel size. Wavelengths of the disturbances were also characterized by the scale of the parcel before collapse.

The pattern of internal gravity waves apparent in figures 5 (*e*) and (*f*) may be better understood by defining rays as straight lines passing through successive crests and troughs of the dye lines. Figure 9 (*a*) shows the progression of the first two troughs and crests below Z_m for a standard experiment. The rays move horizontally away from the collapse region, while their angle, with respect to the vertical, θ, increases. Another feature is that successive rays pass fixed points with approximately the same θ.

Maximum isopycnic displacements occur for rays with θ between approximately 30° and 50°, and can be observed in the probe data presented in figure 10 (*a*). The probes at positions A and B have rays passing with angles of approximately 35° and 50°, respectively, and record relatively large amplitude oscillations with a frequency near $0{\cdot}7N$. The probes at positions C and D record relatively weak oscillations owing partially to the fact that probes C and D are farther from the source than A and B, but predominantly owing to the angular dependence of the wave amplitude.

The ordinate scale for the probe is the displacement ξ, where (3.1) has been used to relate density fluctuations to displacements. Direct measurement of dye line displacements near the probe position agreed to within 20 % of the computed value of ξ. This was considered consistent given the uncertainties in reading the dye line displacements and the validity of the linear expression (3.1).

The internal gravity wave energy propagating down and away from the collapse region was estimated and compared with the difference between the initial and final potential energy of the mean state. Potential energy was defined as

$$P \equiv g \iint_{\text{Tank}} z\rho(x,z)\,dz, \tag{3.2}$$

where $\rho(x,z)$ was the total density field. The initial state was taken as a linear profile plus a small rectangular area of dense parcel fluid. That is,

$$\rho_i(x,z) = \rho_p, \quad -l_0 < x < +l_0, \quad 0 < z < l_0$$

$$\rho_i(x,z) = \rho_0 + \frac{d\rho_a}{dz} z, \quad \text{otherwise.}$$

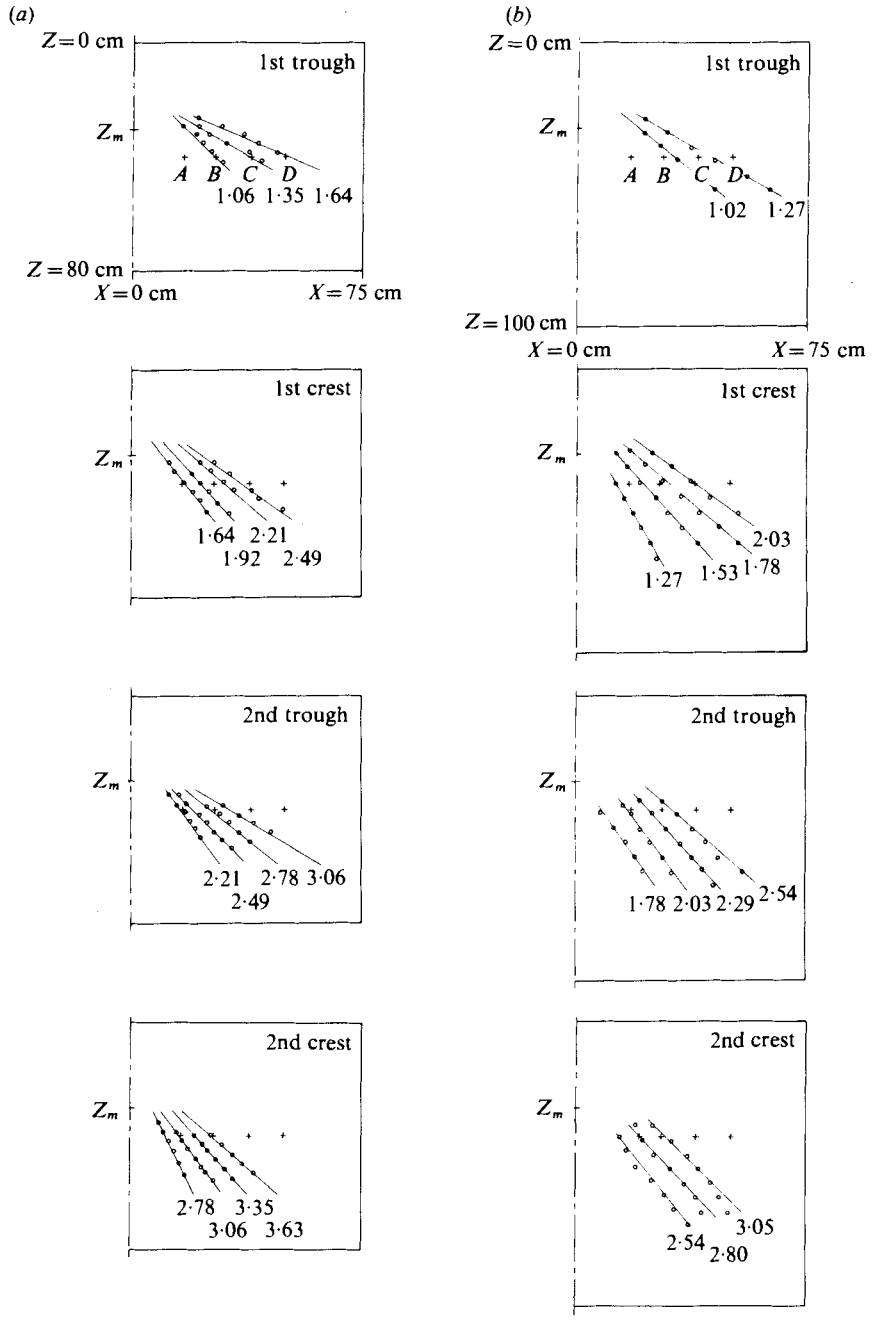

FIGURE 9. (*a*) depicts rays, defined as straight lines connecting troughs and crests of isopycnics, as they propagate away from the parcel collapse region. Rays from the first two troughs and crests are shown and the times are given in units of buoyancy period T. Data in (*b*) are similar to those in (*a*) except that results were derived from numerical experiment.

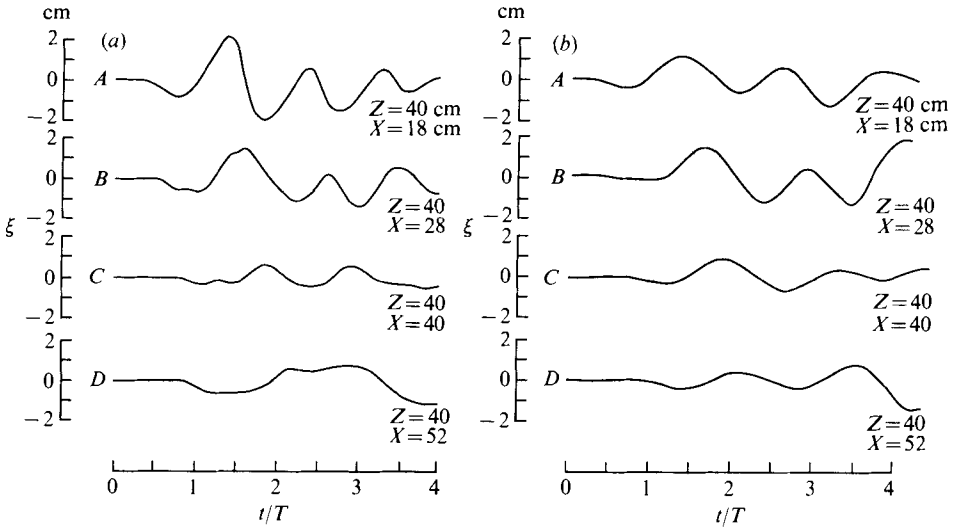

FIGURE 10. (*a*) Data give isopycnic displacement at positions labelled *A* to *D* in figure 9 as a function of normalized time from laboratory experiment. (*b*) Data similar to those in (*a*) except that results were derived from numerical experiment.

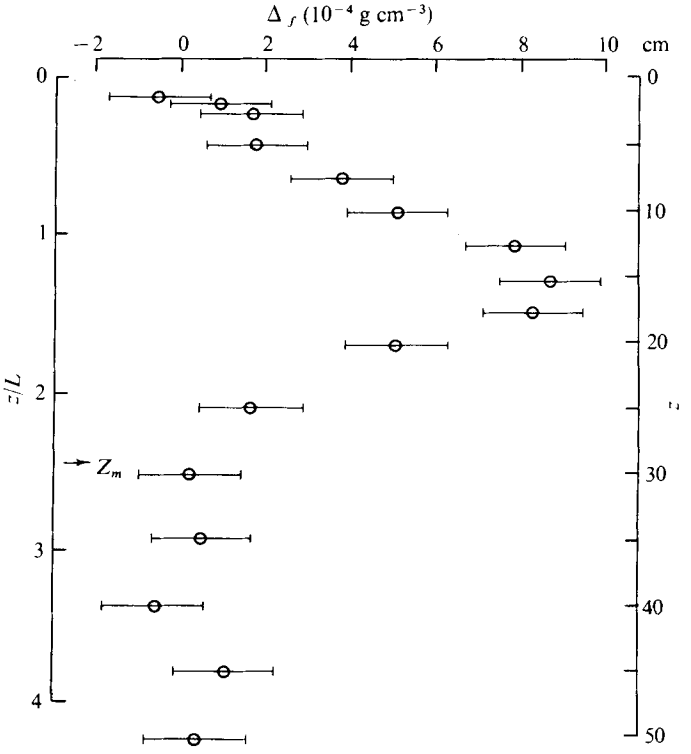

FIGURE 11. Δ_f as a function of vertical position from laboratory experiment. Vertical scale is in units of L and the maximum frontal position Z_m is given.

The final state was taken well after the parcel release when all fluid motions had ceased. This state was found to be independent of x and is given in figure 11. The line stratification was subtracted from the total density, so that Δ_f is defined as

$$\Delta_f(z) \equiv \rho_f(z) - \rho_0 - \frac{d\rho_a}{dz} z,$$

and Δ_f may be approximated by a Gaussian distribution centred at Z_c. Straightforward evaluation of (3.2) for the initial and final states yields

$$P_F - P_I \simeq \Delta m g Z_c,$$

where $\Delta m (\equiv \rho_0 B_0 A_0)$ is the parcel mass and we take $Z_c \gg l_0$.

The potential energy per unit volume of internal gravity waves, $p(x, z)$, in a linearly stratified fluid is given by

$$p(x, z) = \frac{\rho_0 N^2}{2} \xi^2(x, z),$$

where $\xi(x, z)$ is the displacement field. The wave energy may be estimated by the following calculation for the experiment of figure 5. The ray pattern is most pronounced approximately $2T$ after the parcel release. The maximum isopycnic displacement along the rays is approximately 2 cm, while the horizontal and vertical extents of the rays are about 20 and 50 cm, respectively. The average displacement is taken as 1 cm, and the wave potential energy per unit breadth, P_w, is approximated by

$$P_w \simeq 2(\rho_0 N^2/2)\,(1\text{ cm})\,(20 \times 50\text{ cm}^2),$$

$$P_w \simeq 8 \times 10^2 \text{ergs/cm}.$$

The change in parcel potential energy per unit breadth is

$$P_p = g \Delta m Z_c = 2{\cdot}0 \times 10^4 \text{erg/cm}, \tag{3.3}$$

which gives

$$P_w / P_p \simeq 0{\cdot}05.$$

The kinetic plus potential wave energy, E_w, is given as twice P_w (by use of the virial theorem), so that

$$E_w / P_p \sim 10\,\%.$$

It must be emphasized that this is the wave energy at a particular instant, and not the total wave energy radiated away from the collapse region. As two or three sets of rays emanating from the collapse region can typically be discerned, the total wave energy radiated was approximately 20–25 % of P_p.

4. Theoretical discussion

Parcel in a homogeneous fluid

The experimental results for parcel motion in a homogeneous and linearly stratified fluid will be discussed in terms of a simple entrainment model due to Morton *et al.* (1956), and, more recently, Escudier & Maxworthy (1973). This model assumes that:

(i) Ambient fluid is entrained into the parcel at a rate proportional to its area and velocity. The constant of proportionality $\alpha (> 0)$ is the entrainment coefficient.

(ii) The parcel initially has zero impulse and a circular shape, of radius $r(t)$, and all fluid and flow properties are uniformly distributed within it.

(iii) Buoyancy is conserved during the entrainment process and there is no loss of buoyancy or momentum to a wake. Using these assumptions, the equations for conservation of mass, momentum and buoyancy are:

$$\frac{d}{dt}[\pi\rho_p r^2] = 2\pi r\alpha w\rho_0, \tag{4.1}$$

$$\frac{d}{dt}[(1+\gamma)\rho_p \pi r^2 w] = \pi r^2(\rho_p - \rho_0)g, \tag{4.2}$$

$$\frac{d}{dt}[(\rho_p - \rho_0)\pi r^2] = 0. \tag{4.3}$$

ρ_p and ρ_0 are the parcel and ambient densities, respectively, while γ is the inertial coefficient. The quantity $\gamma\pi r^2\rho_0$, known as the virtual mass, represents the added inertia of the parcel due to induced motions in the ambient fluid. Straightforward manipulation (see Escudier & Maxworthy 1973) of these equations yields the following solution for the parcel vertical position z:

$$\zeta_T^{\frac{3}{4}} = k_T t^{\frac{3}{4}},$$

$$\zeta_T \equiv z/(gB_0A_0)^{\frac{1}{4}},$$

$$z\alpha = r - r_0,$$

$$k_T = \left(\frac{3}{2\pi\alpha^2(1+\gamma)}\right),$$

where $A_0 = \pi r_0^2$ is the initial parcel area, and $\rho_0 B_0$ is the initial parcel density excess.

The theoretical slope, k_T ,may be compared with the experimental value by taking $\gamma = 1$ (the value appropriate for a rigid cylinder of *constant* radius) and $\alpha = 0{\cdot}55$. This yields

$$k_T = 0{\cdot}89,$$

compared with

$$k_E = 0{\cdot}78,$$

which represents an agreement between theory and experiment of better than 15 %. This agreement is better than one might expect given the simplicity of the model and the difficulty in rigorously justifying the entrainment assumption (see Escudier & Maxworthy 1973, §4) and using the rigid cylinder value of $\gamma = 1$.

Parcel in a linearly stratified fluid

The same assumptions previously given can be used to model the parcel motion in a linearly stratified fluid, and the model is basically that of Morton *et al.*, with the addition of a virtual mass term in the momentum equation. The assumption that the parcel retains its circular shape is approximately valid until the time of maximum depth, and completely invalid after this time. The equations of mass, momentum and buoyancy conservation are

$$\frac{d}{dt}[\rho_p \pi r^2] = 2\pi\alpha|w|\rho_a, \tag{4.4}$$

$$\frac{d}{dt}[(\rho_p \pi r^2 + \gamma \rho_0 \pi r^2) w] = g\pi r^2(\rho_p - \rho_a), \tag{4.5}$$

$$\frac{d}{dt}[(\rho_p - \rho_a)\pi r^2] = -\pi r^2 w \frac{d\rho_a}{dz}. \tag{4.6}$$

Combining (4.4) and (4.6) yields the familiar result

$$r - r_0 = \alpha z, \tag{4.7}$$

where z is the vertical midpoint of the parcel. A scale height is defined as

$$H \equiv \frac{\rho_0}{d\rho_a/dz},$$

and the following approximations are made

$$r \gg r_0,$$

$$Z/H \ll 1,$$

$$r/H \ll 1$$

(H was typically 1500 cm). Combining all three conservation equations with use of the above approximations gives

$$\ddot{z}z^2 + 2z\dot{z}^2 = \frac{gB_0A_0}{\alpha^2(1+\gamma)} - \frac{N^2z^3}{3(1+\gamma)}, \tag{4.8}$$

and the solution to (4.8) is

$$z = \left(\frac{3}{\pi\alpha^2}\right)^{\frac{1}{3}} L\left(1 - \cos\frac{Nt}{(1+\gamma)^{\frac{1}{2}}}\right)^{\frac{1}{3}},$$

where $L \equiv (gB_0A_0/N^2)^{\frac{1}{3}}$. This solution predicts that the parcel centre reaches a maximum depth of $(6/\pi\alpha^2)^{\frac{1}{3}} L$ in a time $\frac{1}{2}(1+\gamma)^{\frac{1}{2}} T$. Substituting the values $\alpha = 0{\cdot}55$ and $\gamma = 1$ yields that

$$Z_{\text{centre}} = 1{\cdot}9L,$$

and is reached in a fall time equal to

$$T_{\text{fall}} = 0{\cdot}7T.$$

Both quantities agree remarkably well with the experimental values of $Z_c = 1{\cdot}8L$ attained in a time of $0{\cdot}7T$. This agreement must be viewed cautiously, however, given the simplicity of the model.

Internal gravity waves

The ray pattern observed experimentally (figure 9) arises from a complicated forcing due to the parcel motion. Although no theory for this generation process is presented, a few remarks can be made. It is well known that oscillating a rigid body in a linearly stratified fluid at frequency $\omega_s (< N)$ will excite internal gravity waves with the same frequency and wavelengths characterized by the size of the body. The pattern for such waves will be one of the maximum isopycnic displacement along rays with an angle θ to the vertical given by

$$\theta = \cos^{-1}\frac{\omega_s}{N}.$$

The ray pattern observed in this study shows maximum isopycnic displacement for angles between 30° and 50° from the vertical. This is consistent with frequencies near

$0{\cdot}7N$ (or periods near $1{\cdot}4T$) being dominant. This period can be explained in terms of the parcel fall time by assuming that the fall time of $0{\cdot}7T$ represents one half-period of the forcing. In this way, the dominant period of internal wave oscillations is a natural consequence of the parcel motion.

The increase in θ as the rays move away from the source may be explained by an argument from Wu (1969). The parcel excites a spectrum of wavelengths and the phase and group velocity of internal waves increases with increasing wavelength. Therefore, crests and troughs farthest from the source are associated with the longest wavelengths, while those near the source are associated with shorter wavelengths. This speed difference will result in the rays connecting crests and troughs increasing their angle to the vertical as time progresses.

5. Numerical experiments

Model description

A numerical model to simulate the dynamics of internal gravity waves and penetrative convection was developed by Orlanski & Ross (1973), and used to simulate the laboratory experiments of parcel motion in both the homogeneous and the stratified cases. A brief description of the model will be given here and the reader is referred to Orlanski & Ross for a more detailed description.

The model simulated two-dimensional flow in a rectangular container where temperature was used to produce the density variations. The horizontal and vertical grid spacings were 2 and 1 cm, respectively, and the fluid motion and temperature field were assumed to be symmetric about a vertical line passing down the middle of the tank. The calculations were carried out for only the right-hand side of the tank, with the left and right boundaries of the calculation corresponding to the tank centre-line and right wall, respectively. The actual tank dimensions modelled were 160 cm long by 100 cm deep. Symmetry conditions were used along the right wall, while conditions of zero normal velocity and tangential stress were applied at the rigid walls, along with adiabatic conditions for the perturbation temperature.

The key aspect of this model is the parameterization of sub-grid scale turbulence. The scheme provides large diffusivities of heat and momentum in regions where unstable gradients exist, and small background diffusivities where the flow is gravitationally stable. The turbulent Prandtl number, $Pr = \nu/k$, is taken as unity, where k and ν are diffusivities of momentum and heat, respectively. The diffusivity ν in a given grid box is calculated as

$$\nu = \nu_0, \quad \Delta T \geqslant 0,$$

$$\nu = \nu_0\left[1 + K\left[\frac{g\Delta T}{T\nu_0^2}\right]^{\frac{1}{3}}\Delta z\right], \quad \Delta T < 0,$$

where ν_0 is the molecular diffusivity of fresh water, T is the temperature, ΔT is the temperature difference across the vertical grid spacing Δz, and K is an adjustable constant. This scheme implies a non-dimensional heat and momentum flux proportional to a Rayleigh number raised to the one-third power when $\Delta T < 0$. This becomes apparent by rewriting the above as

$$\nu = \nu_0[1 + KRa^{\frac{1}{3}}], \quad \Delta T < 0,$$

where $$Ra = \frac{g\Delta\theta\Delta z^3}{\Theta k_0 \nu_0}$$

is a Rayleigh number based on the grid box dimensions. A detailed discussion of the theoretical and experimental justification of this assumption is given by Orlanski & Ross (1973). The numerical results were fairly insensitive to the value of K over a range of 5 to 15, with $K = 15$ providing the best simulation of the laboratory experiment. It should be mentioned that the Prandtl number for molecular diffusivities was taken to be unity for convenience and resulted in greatly overestimating the molecular diffusivity of heat. This does not cause any significant error, as ν_0 is small enough to make the simulation virtually non-diffusive where the field is gravitationally stable.

Parcel in a homogeneous fluid

The numerical integration began with a constant ambient temperature and a cold region near the upper right corner of the calculation field, which was equivalent to a parcel measuring 8 cm long by 2 cm deep in a full tank. The parcel was 27 °C colder than the surrounding fluid and its centre was 7 cm from the free surface. This differs from the laboratory experiments, but was necessary, as placing the initial parcel too near the free surface resulted in large vertical gradients of temperature and velocity which were poorly resolved. The results of the simulation are given in figure 12 and figures 4(*c*) and (*d*).

Figure 12 shows the numerical simulation of streak photography. The stippled region represents a temperature anomaly of greater than 0·02 °C and is analogous to the dye region in figure 3. The integration (or 'exposure') time was $\frac{1}{2}$ s. A comparison of the laboratory and experimental results shows qualitative agreement between the two. In both cases, the dye region grows with increasing depth and a vortex pair can be discerned. A more quantitative comparison between the two experiments is made in figure 4. Parcel radius r_N is plotted versus vertical position z_N [see figure 4(*c*)] and the variable $\zeta_N^{\frac{3}{2}}$ ($\zeta_N \equiv z_N/(gB_0A_0)^{\frac{1}{3}}$) is plotted versus time [figure4(*d*)]. The slope $\Delta r_N/\Delta z_N$ of approximately 0·5 agrees well with the experimental value of 0·55. The rate of parcel descent, given by the slope k_N of $\zeta_N^{\frac{3}{2}}$ versus time, is approximately

$$k_N = 0{\cdot}71,$$

compared with the experimental value of 0·78. This implies that the model simulates the growth of the parcel via the entrainment of ambient fluid accurately, but not the parcel's velocity.

This discrepancy is believed to be related to resolution problems during the initial stages of the parcel's acceleration. The simple entrainment model of Escudier & Maxworthy predicts that the parcel accelerates until a time of about $\frac{1}{2}(r_0/\alpha g B_0)^{\frac{1}{2}}$, or about 0·1 s for the present study. It is during this stage that the large scale circulation of the vortex pair is developing and the grid spacing of $\Delta x = 2$ cm and $\Delta z = 1$ cm is probably not fine enough to model this process accurately. Experiments on parcel motion in a stratified fluid showed that for times greater than $\frac{1}{2}(g/\alpha g B_0)^{\frac{1}{2}}$ but well before the parcel reached maximum vertical position, the vertical velocities increased with decreasing horizontal grid size ($\Delta x = 4, 2, 1$ cm). The spacing of $\Delta x = 1$ cm would have been desirable, but would have required a prohibitive amount of computer memory.

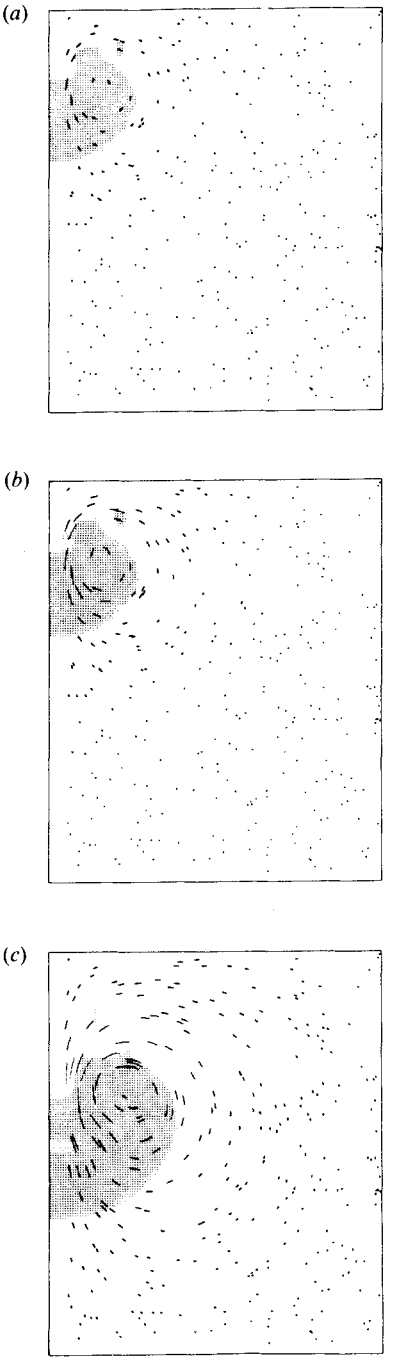

FIGURE 12. Numerical simulation of streak and dye photography for parcel motion in a homogeneous fluid. (*a*) t = 1–1·5 s; (*b*) t = 2–2·5 s; (*c*) t = 3–3·5 s. B_0A_0 = 1·36.

Parcel kinetic and potential energies were defined as

$$\text{K.E.} = \tfrac{1}{2}\rho_0 \iint (u^2 + w^2)\, dx\, dz,$$

$$\text{P.E.} = g \iint (\rho(x,z) - \rho_0)\, z\, dx\, dz,$$

where the integration was taken over the entire tank and $\rho(x,z)$ was the total density field. It was found that both the kinetic energy and the change in potential energy were proportional to $t^{\frac{2}{3}}$ for times greater than about 2 s. The kinetic energy was approximately 50 % of the change in potential energy, with the difference being dissipated via sub-grid scale parameterization. This result is consistent with numerical studies by Lilly (1962, 1964) and experimental results of Richards (1963), who estimated that between 22 and 58 % of the potential energy released was transformed into mean motion.

Parcel in a linearly stratified fluid

The initial conditions of the previous section were applied in a linearly stratified ambient fluid of temperature gradient 0·187 °C cm^{-1} (buoyancy period $T = 7{\cdot}66$ s). This set of conditions approximates a standard laboratory experiment. A tracer field was included in the initial parcel which was advected and mixed by the parcel motion, and simulated the presence of dye in the laboratory experiments.

Results from the numerical simulation are presented in figure 13, where the format is similar to that of figure 5. The stippled area represents the tracer field, while the horizontal lines are isotherms (isopycnics). A comparison of figures 5 and 13 reveals that qualitative features of the two experiments are similar. Parcel size and depth as a function of time agree fairly well, as does the pattern of internal waves emanating from the collapse region. Quantitative data from the numerical experiment will now be presented.

The passage of the parcel can be observed in the temperature records given in figure 7(*c*). The records were taken along the symmetry axis ($x = 0$) and at 6, 12, 15 and 18 cm from the initial parcel. The last two points differ from those of the laboratory data; this was done because the maximum parcel depth in the numerical experiment was less than that observed in the laboratory experiment. This resulted in the numerical positions of 15 and 18 cm being approximately equivalent to the experimental depths of 18 and 24 cm. The temperature data has been converted to density to match the scales used for the laboratory data.

The signals at the first two positions show the passage of cold, dense fluid, followed by light fluid advected into the region by the vortex motion. The magnitude of the maximum density excess at the 6 cm position is less than that observed in the laboratory experiment, this being a consequence of the difference in initial conditions. The initial parcel was 25 % lighter than the experimental parcel, although it was 25 % larger to produce equal values of $B_0 A_0$ for the two types of experiment. The duration of the signal due to dense fluid is somewhat greater in the model than for the laboratory experiment, and this can in part be attributed to differences in initial conditions. The magnitude and duration of the signal due to the dense parcel fluid agree fairly well with the laboratory data at the 12 cm level, and at this point, the differences in initial conditions appear to be lost. One striking difference between the laboratory and numerical

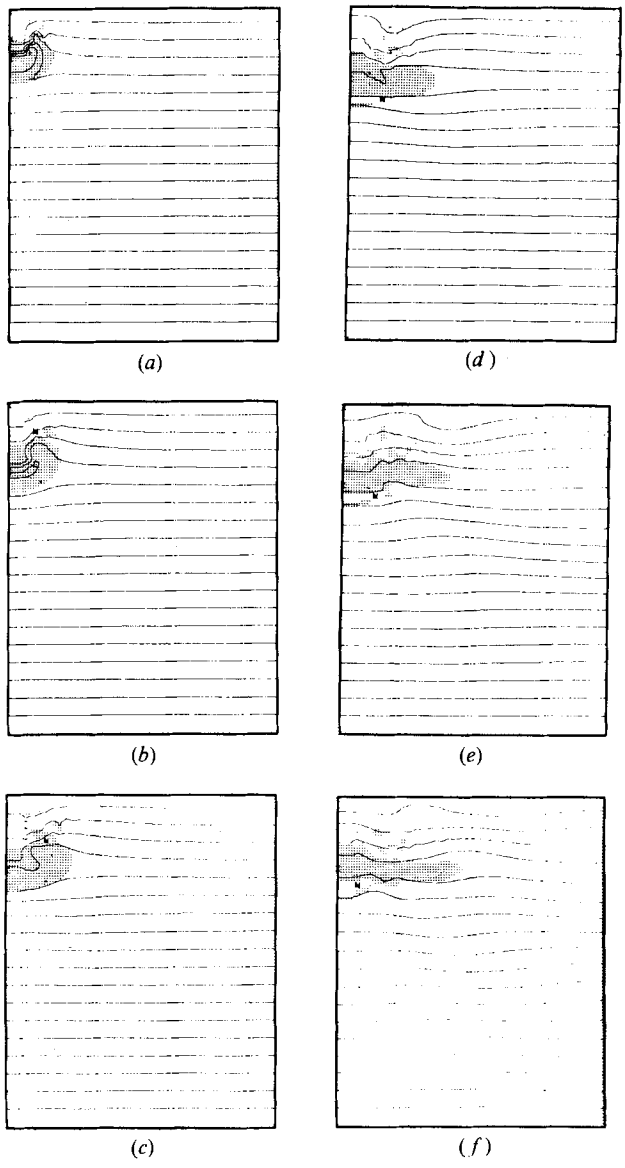

FIGURE 13. Numerical simulation of parcel motion in a linearly stratified fluid. The stippled area represents a tracer field analogous to dye in the laboratory experiments, while the horizontal lines are isopycnics. The times chosen are identical to those of the laboratory data in figure 5. (*a*) $t = 0{\cdot}26T$; (*b*) $t = 0{\cdot}44T$; (*c*) $t = 0{\cdot}70T$; (*d*) $t = 0{\cdot}96T$; (*e*) $t = 1{\cdot}84T$; (*f*) $t = 2{\cdot}45T$.

results is the 'sharpness' of the dense fluid signal in the laboratory experiment, as compared with the more gradual density increase observed in the model. This difference is a consequence of the resolution of the numerical model. The interface between parcel and ambient fluid is of the order 1 cm or less, and the vertical resolution of 1 cm cannot be expected to resolve this interface precisely. The signal at the third level shows that the parcel fluid has now been greatly diluted, and the signal due to dense fluid is approximately equal in magnitude to the signal due to the advection of lighter ambient

fluid. The signal at the lowest position results entirely from the downward displacement of isopycnics ahead of the parcel.

The front position of the parcel tracer with respect to the initial parcel is given as a function of time in figure 8(*b*) along with the temperature record slightly below (~ 2 cm) the deepest tracer position. The model parcel reaches maximum depth at approximately $0{\cdot}65T$ after release and subsequent oscillations at twice this interval (between $1{\cdot}2$ and $1{\cdot}4T$) can be observed in both numerical records, which is in good agreement with the laboratory results. The maximum depth of the parcel in the simulation is about 25 % less than that observed experimentally ($1{\cdot}8L$, compared with $2{\cdot}5L$). This is believed to be a resolution problem, as discussed previously. The initial acceleration stage of the parcel's motion is not accurately modelled, and this results in smaller velocities and penetration depths than are observed in the laboratory.

Ray-like patterns emanating from the parcel region were observed in the numerical experiment similar to those seen in the laboratory study, and are presented in figure 9(*b*). The general behaviour of the rays, which increase their angle to the vertical as they propagate away from the collapse region, is similar to that observed experimentally and the explanation is the same as that given in §4. Inspection of the data shows that the rays in the simulation move about 10 to 20 % more rapidly than is observed experimentally, and may be a consequence of the slightly higher frequencies observed in the model relative to the laboratory study ($\sim 0{\cdot}8N$ numerical, as compared to $0{\cdot}7N$ laboratory). For times greater than about $2{\cdot}5T$, the effects of reflexions were observed in the ray patterns. Although not shown in figure 9, ray patterns aligned nearly with the vertical started to become apparent in the lowest portion of the tank. This was the result of reflexions and the build-up of standing wave patterns. Similar behaviour could be observed in the laboratory study, although not as clearly. Standing patterns were less apparent for the laboratory results owing to the wave absorbers and the lack of precise symmetry which reduce interference effects.

Temperature records from the four positions labelled A to D are presented in figure 10(*b*). The maximum amplitudes were observed at positions A and B, where the rays passed with angles equal to approximately 35° and 50°, respectively. This result is consistent with dominant oscillation frequencies of approximately $0{\cdot}8$ and $0{\cdot}7N$, and the explanation for the relative magnitude of the waves at the four positions is the same as discussed in §4.

The above discussion shows that the numerical model simulates the laboratory experiment fairly accurately, both for the parcel motion and generation of internal gravity waves. Results from the model experiment may be used to discuss the energetics of waves propagating out from the collapse region. It was found that wave energy enters the lower portion of the tank, and continues to build up in this region while reflexions from the rigid wall result in the formation of a standing pattern. This arrangement is not an ideal one for calculating the total wave energy radiated away from the parcel, but can be used by assuming that the wave energy observed from this standing pattern is a good approximation to the total energy radiated downward.

The wave kinetic and potential energies per unit width are defined as

$$K_w = \frac{\rho_0}{2}\int\int (u^2+w^2)\,dx\,dz,$$

$$P_w = \frac{\rho_0 g^2}{2N^2}\int\int \left(\frac{\Delta\rho}{\rho_0}\right)^2 dx\,dz,$$

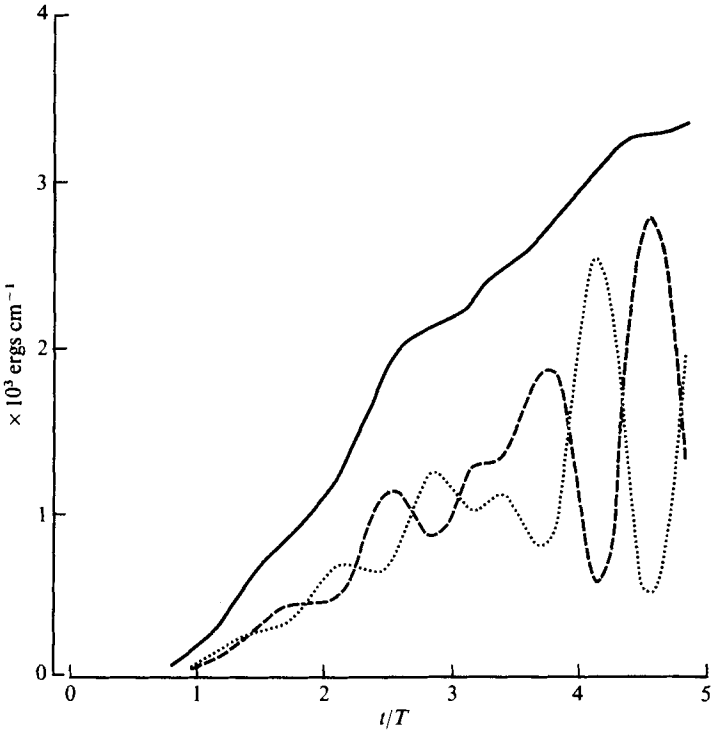

FIGURE 14. Potential and kinetic energy per unit breadth of the tank as a function of normalized time for the lowest 60 cm of the tank; data from numerical simulation. ·····, P_W; – – –, K_{00}; ——, $E_W = P_W + K_W$.

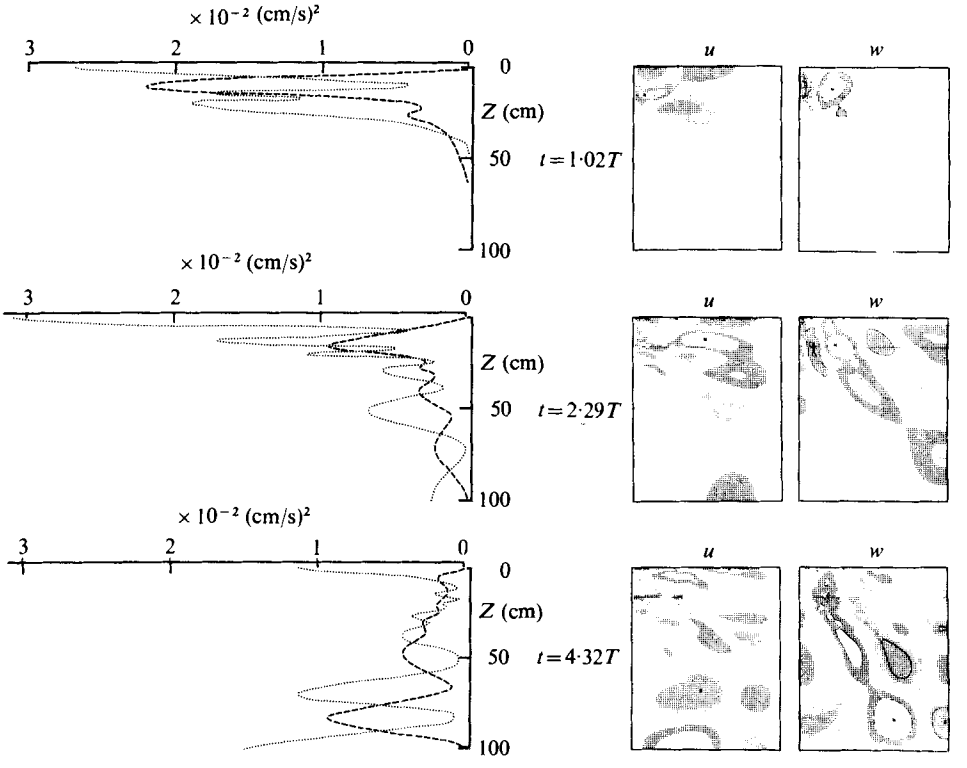

FIGURE 15. Horizontally averaged horizontal and vertical velocities as a function of vertical position are given along with contour plots of u and w at three times. Data show the propagation of kinetic energy downward as time progresses. ·····, $\overline{u^2}$; – – –, $\overline{w^2}$.

where $\Delta\rho$ is the density deviation from ambient. E_w and P_w are plotted as a function of time in figure 14 along with their sum, for the lowest 60 cm of the tank. During the time of parcel descent and collapse, very little wave energy is observed in this region, but a short time after parcel collapse ($t \sim 1{\cdot}0T$), energy begins to enter the region. Wave energy continues to grow in this region until $t \sim 5{\cdot}0T$, when a fairly energetic standing mode can be observed in the region of interest. It is this maximum value of wave energy which will be used to estimate the total wave energy resulting from the parcel collapse.

The behaviour described above may also be observed in figure 15, where the horizontally averaged values of u^2 and w^2 are plotted as a function of depth at three times along with contour plots of u and w. The first time, $t = 1{\cdot}02T$, is near the time of parcel collapse, while $t = 2{\cdot}29T$ and $4{\cdot}32T$ are times of relative maxima for the kinetic energy. At $t = 1{\cdot}02T$, the kinetic energy is due to the parcel motion and is concentrated in the upper portion of the tank. By the intermediate time, wave kinetic energy may be observed in the lower portion of the tank, with a dominant vertical wavelength of approximately 60 cm. An intensification of $\overline{u^2}$ also occurs near the top of the tank, which appears to be the result of energy propagated upward from the collapse area. At the final time, the kinetic energy in the lower portion of the tank is a maximum. This behaviour is also evident in the contour plots, and inspection of the data shows that the dominant wavelengths are approximately 60 to 80 cm. Although these lengths are of the order of tank dimensions, they are determined by the parcel forcing and not the tank boundaries. Parcel size before collapse was approximately 25 cm, and this was most effective in generating waves with a scale 2 to 3 times parcel size. This scale selection was evident in the comparison of the present results with an experiment where maximum parcel depth (and therefore size) was about 30 % greater. In that case, the vertical structure was dominated by a mode with a vertical wavelength of 100 cm, compared with 60 cm in the present study.

The maximum wave energy in the lower portion of the tank can be compared with the change in parcel potential energy, P_p. This change in energy is

$$P_p = 1{\cdot}77 \times 10^4 \text{erg/cm},$$

which is equivalent to the mass excess of the parcel falling approximately 12 cm [see (3.3)]. The maximum wave energy is found to be approximately

$$E_w = (K_w + P_w) = 0{\cdot}32 \times 10^4 \text{erg/cm},$$

so that

$$\frac{E_w}{P_p} = 0{\cdot}18.$$

As E_w is the wave energy in the lowest 60 cm of the tank, the above estimate is a low one. Given this, the result is consistent with the value of $E_w/P_p \sim 20$–25 % estimated from the laboratory data.

6. Discussion

Laboratory and numerical experiments were conducted to study the motion of two-dimensional parcels in both a homogeneous and a linearly stratified fluid. The laboratory findings for the homogeneous case were consistent with the previous work

of Scorer (1958) and Richards (1963); the parcel grew linearly with vertical position z and z increased as time raised to the two-thirds power. The laboratory results were interpreted in terms of the entraining parcel model given by Escudier & Maxworthy, and good agreement was found between this simple theoretical model and the experimental findings.

Numerical experiments using a model developed by Orlanski & Ross (1973) yielded results very similar to those obtained in the laboratory. The parcel growth rate with respect to vertical position agreed well with laboratory results, while the descent rate was about 10 % less than that observed. This discrepancy was most likely due to resolution problems during the earliest stages of the parcel motion. The key aspect of the numerical model was a scheme for parameterizing sub-grid scale mixing when statically unstable density gradients were present. The method was essentially one with the eddy diffusivity proportional to $Ra^{\frac{1}{3}}$, where Ra was a Rayleigh number based on the vertical grid spacing and temperature difference across that spacing. This method appeared to be well suited for the case of the entraining parcel, where ambient fluid is mixed into the parcel at the statically unstable front and advected into the back of the parcel via the vortex pair motion.

The laboratory experiments with a linearly stratified fluid demonstrated the significant effects of stratification upon the parcel motion, with the obvious feature being that the parcel could attain an equilibrium position. It was also observed that the response of the ambient fluid collapsed the parcel and that the parcel motion generated internal gravity waves. The entraining parcel model discussed by Morton *et al.* (1956) was modified by the addition of a virtual mass term and found to agree remarkably well with the laboratory results. This agreement may well be fortuitous, as the model possibly neglects some of the physics. It is known from the work of Warren (1960) that a drag will be experienced by a parcel owing to the generation of internal gravity waves, and no such mechanism was included in the simple model used. It is possible that just as all the physics of turbulent entrainment are contained in the entrainment coefficient α, a good deal of physics may be hidden in the virtual mass coefficient.

The internal waves generated by the parcel motion were characterized by periods of approximately twice the parcel fall time and wavelengths of about two to three times the parcel size before collapse. A spectrum of wavelengths was excited and accounted for the observed ray pattern emanating from the collapse region. The energy radiated away from this region was estimated to be about 20–25 % of the potential energy released through the parcel's falling.

The numerical experiment yielded similar behaviour to that observed in the laboratory, although the maximum parcel depth was about 20 % less than that observed and was reached slightly more quickly ($0{\cdot}65T$ compared with $0{\cdot}70T$). The model also showed internal waves characterized by periods of twice the fall time and wavelengths of about two to three times parcel size before collapse.

An example in nature of penetrative convection into a stably stratified fluid is cumulus convection during severe storms. Typically, these storms consist of several cells with updraft regions about 2 to 8 km wide. Indications are that a well-developed cell is dominated by a continuous 'plume-like' updraft, whereas 'bubbles' or discrete parcels of buoyant air may dominate the formative stages of the cell (Newton 1967). The motion of such 'bubbles' may have been the mechanism responsible for the internal waves observed at ground level by Kjelass *et al.* (1975). They found waves

with dominant periods and phase speeds of about 14 min and 10 m/s, respectively, which yields a wavelength of about 8 km. This wave activity was believed to be associated with a convective storm some 100 km away. Taking typical updraft velocities as 20 m/s and cloud tops at 12 km, the rise time for 'bubbles' is about 10 min, while the size of individual bubbles is somewhat less than typical cell widths.

Another application of the present results relates to the work of Linden (1973, 1975), who found that the turbulent eddies in a mixed layer may be described as vortex rings. The impacting of such eddies upon a density jump overlying a linearly stratified region was very effective at generating internal waves. The density jump was great enough to halt the eddies at this interface, but in situations where the density jump is weak, individual eddies may penetrate into the linearly stratified region and excite waves in a manner similar to that observed in the present study.

The author wishes to thank Dr I. Orlanski of the Geophysical Fluid Dynamics Laboratory for proposing this study and his guidance through all aspects of the work, while Dr B. Ross and Mr L. Polinsky were both very helpful in regard to the numerical computation. She also thanks Mr B. Williams and Mrs C. Longmuir for typing the manuscript. This work was supported by the Geophysical Fluid Dynamics Laboratory/NOAA under Grant 04-3-022-33.

REFERENCES

Delisi, D. P. & Orlanski, I. 1975 On the role of density jumps in the reflexion and breaking of internal gravity waves. *J. Fluid Mech.* **69**, 445–464.

Escudier, M. P. & Maxworthy, T. 1973 On the motion of turbulent thermals. *J. Fluid Mech.* **61**, 541–552.

Fortuin, J. M. H. 1960 Theory and application of two supplementary methods of constructing density gradient columns. *J. Polymer Sci.* **44**, 505–515.

Kjelaas, A. G., Gossard, E. E., Young, J. M. & Moninger, W. R. 1975 Dispersion and spectra of gravity waves probably generated by a convective storm. *Tellus* **27**, 25–32.

Lilly, D. C. 1962 On the numerical simulation of buoyant convection. *Tellus* **14**, 148–172.

Lilly, D. C. 1964 Numerical solutions for the shape-preserving two-dimensional thermal convection. *J. Atmos. Sci.* **21**, 83–98.

Linden, P. F. 1973 The interaction of a vortex ring with a sharp density interface: a model for turbulent entrainment. *J. Fluid Mech.* **60**, 467–480.

Linden, P. F. 1975 The deepening of a mixed layer in a stratified fluid. *J. Fluid Mech.* **71**, 385–405.

McLaren, T. I., Pierce, A. D., Fohl, T. & Murphy, B. L. 1973 On investigation of internal gravity waves generated by a buoyantly rising fluid in a stratified medium. *J. Fluid Mech.* **57**, 229–240.

Maxworthy, T. & Browand, F. K. 1975 Experiments in rotating and stratified flows: with oceanographic application. *Ann. Rev. Fluid Mech.* **7**, 273–303.

Morton, B. R., Taylor, G. & Turner, J. S. 1956 Turbulent gravitational convection from maintained and instantaneous sources. *Proc. Roy. Soc.* A **234**, 1–23.

Newton, C. W. 1967 Severe convection storms. *Adv. in Geophys.* **12**, 257–308.

Orlanski, I. & Ross, B. B. 1973 Numerical simulation of the generation and breaking of internal gravity waves. *J. Geophys. Res.* **78**, 8806–8826.

Richards, J. M. 1963 Experiments on the motion of isolated cylindrical thermals through unstratified surroundings. *Int. J. Air. Wat. Poll.* **7**, 17–34.

SCORER, R. S. 1957 Experiments on convection of isolated masses of buoyant fluid. *J. Fluid Mech.* **2**, 583–594.

SCORER, R. S. 1958 *Natural Aerodynamics*. Pergamon.

TURNER, J. S. 1964 The dynamics of spheroidal masses of buoyant fluid. *J. Fluid Mech.* **19**, 481–490.

WU, J. 1969 Mixed region collapse with internal wave generation in a density stratified medium. *J. Fluid Mech.* **35**, 531–544.

WARREN, F. W. G. 1960 Wave resistance to vertical motion in a stratified fluid. *J. Fluid Mech.* **7**, 209–229.

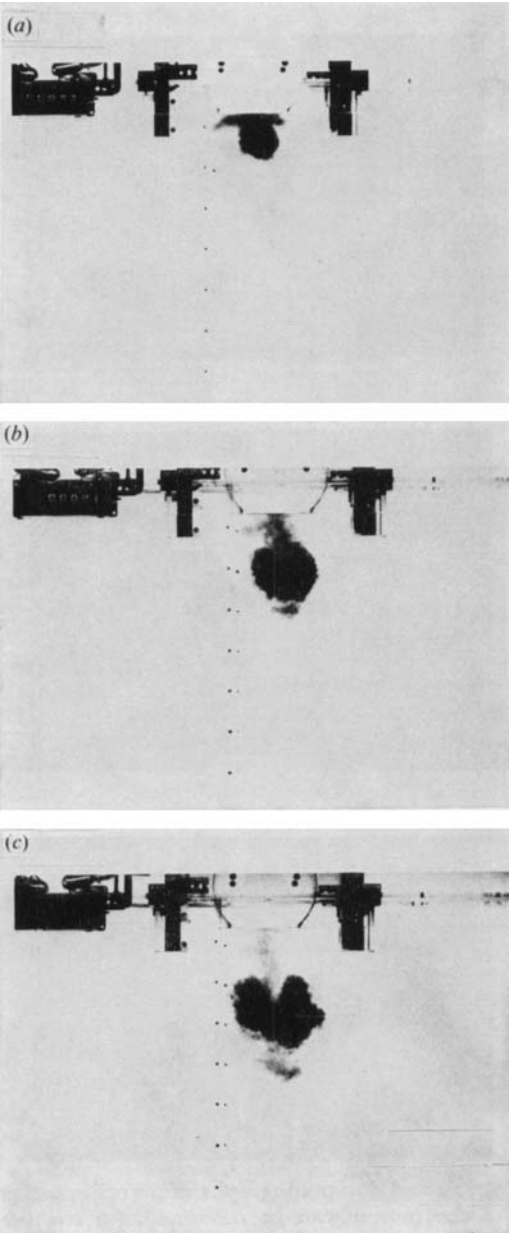

FIGURE 2. Photographs of parcel descent in a homogeneous fluid at three separate times. The parcel can be seen to grow in size as it falls while its shape remains similar. (*a*) $t = 1$ s; (*b*) $t = 3$ s; (*c*) $t = 5$ s. $B_0 = 0{\cdot}042$, $A_0 = 22{\cdot}4$ cm^2.

(*a*)

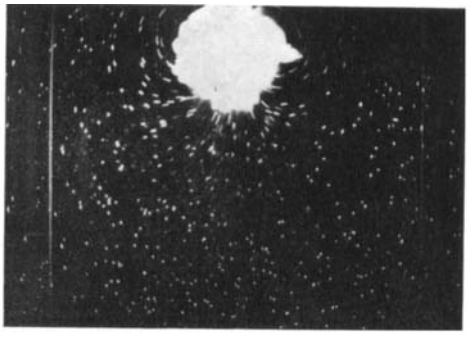

(*b*)

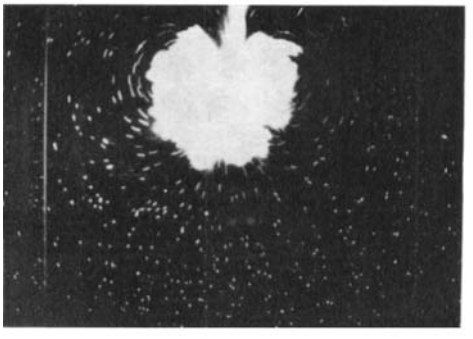

(*c*)

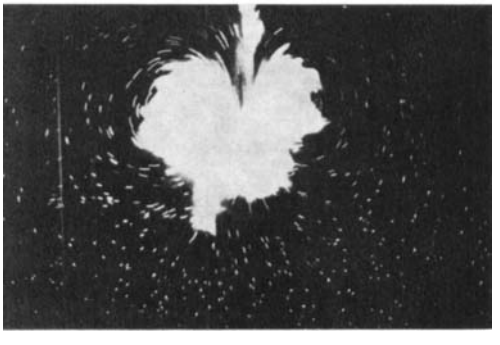

FIGURE 3. Combination streak and dye photographs of parcel in a homogeneous fluid, in which the vortex-pair nature of the motion can be discerned. (*a*) $t = 1{\cdot}0$–$1{\cdot}5$ s; (*b*) $t = 2{\cdot}0$–$2{\cdot}5$ s; (*c*) $t = 3{\cdot}0$–$3{\cdot}5$ s. $B_0 = 0{\cdot}060$, $A_0 = 22{\cdot}4$ cm^2.

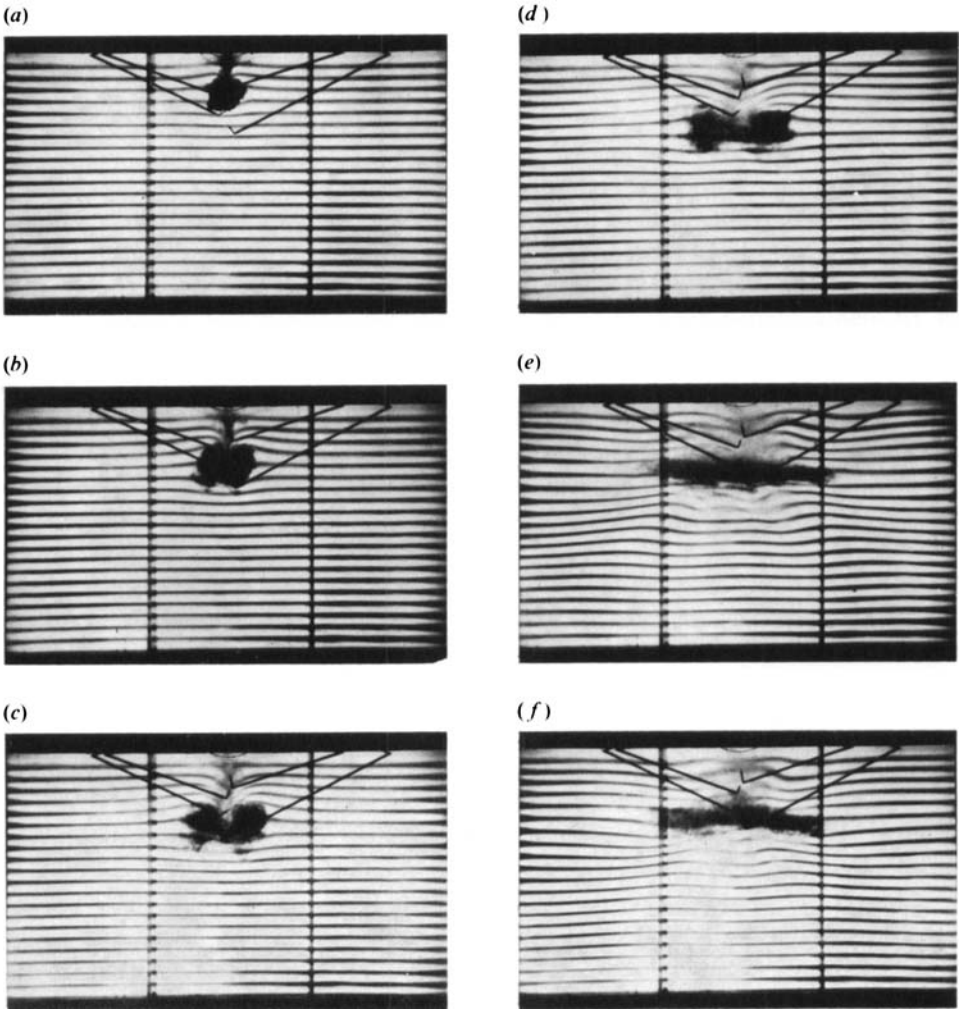

FIGURE 5. Photographs of parcel motion in a linearly stratified fluid. Parcel growth, attainment of maximum position, collapse and subsequent internal wave field can be seen in this sequence of photographs. (*a*) $t = 0{\cdot}26T$; (*b*) $t = 0{\cdot}44T$; (*c*) $t = 0{\cdot}70T$; (*d*) $t = 0{\cdot}96T$; (*e*) $t = 1{\cdot}84T$; (*f*) $t = 2{\cdot}45T$.